



**HAL**  
open science

## Application of Synchrotron Radiation-Based Micro-Analysis on Cadmium Yellows in Pablo Picasso's Femme

Marta Ghirardello, Victor Gonzalez, Letizia Monico, Austin Nevin, Douglas Maclennan, Catherine Schmidt Patterson, Manfred Burghammer, Matthieu Réfrégiers, Daniela Comelli, Marine Cotte

► **To cite this version:**

Marta Ghirardello, Victor Gonzalez, Letizia Monico, Austin Nevin, Douglas Maclennan, et al.. Application of Synchrotron Radiation-Based Micro-Analysis on Cadmium Yellows in Pablo Picasso's Femme. *Microscopy and Microanalysis*, 2022, 28 (5), pp.1504-1513. 10.1017/S1431927622000873 . hal-03711191

**HAL Id: hal-03711191**

**<https://hal.science/hal-03711191v1>**


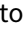







Submitted on 17 Jan 2024

**HAL** is a multi-disciplinary open access archive for the deposit and dissemination of scientific research documents, whether they are published or not. The documents may come from teaching and research institutions in France or abroad, or from public or private research centers.

L'archive ouverte pluridisciplinaire **HAL**, est destinée au dépôt et à la diffusion de documents scientifiques de niveau recherche, publiés ou non, émanant des établissements d'enseignement et de recherche français ou étrangers, des laboratoires publics ou privés.

## Original Article

# Application of Synchrotron Radiation-Based Micro-Analysis on Cadmium Yellows in Pablo Picasso's *Femme*

Marta Ghirardello<sup>1\*</sup> , Victor Gonzalez<sup>2</sup> , Letizia Monico<sup>3</sup> , Austin Nevin<sup>4,5</sup> , Douglas MacLennan<sup>6</sup> , Catherine Schmidt Patterson<sup>6</sup> , Manfred Burghammer<sup>7</sup>, Matthieu Réfrégiers<sup>8,9</sup> , Daniela Comelli<sup>1</sup>  and Marine Cotte<sup>7,10\*</sup> 

<sup>1</sup>Physics Department, Politecnico di Milano, Piazza Leonardo da Vinci 32, 20133 Milano, Italy; <sup>2</sup>Université Paris-Saclay, ENS Paris-Saclay, CNRS, PPSM, 91190 Gif-sur-Yvette, France; <sup>3</sup>CNR-SCITEC, Via Elce di Sotto 8, 06123 Perugia, Italy; <sup>4</sup>IFN-CNR, Piazza Leonardo da Vinci 32, 20133 Milano, Italy; <sup>5</sup>Courtauld Institute of Art, Somerset House, Strand, London WC2R 0RN, UK; <sup>6</sup>Science Department, Getty Conservation Institute, 1200 Getty Center Drive, Los Angeles, CA 90049, USA; <sup>7</sup>ESRF, 71 Avenue des Martyrs, 38000 Grenoble, France; <sup>8</sup>Synchrotron SOLEIL, L'Orme des Merisiers, Saint-Aubin, Gif-sur-Yvette, France; <sup>9</sup>CBM UPR4301, Rue Charles Sadron, Orléans, France and <sup>10</sup>LAMS, CNRS UMR 8220, Sorbonne Université, UPMC Univ. Paris 06, Place Jussieu 4, F-75005 Paris, France

## Abstract

The cultural heritage community is increasingly exploring synchrotron radiation (SR) based techniques for the study of art and archaeological objects. When considering heterogeneous and complex micro-samples, such as those from paintings, the combination of different SR X-ray techniques is often exploited to overcome the intrinsic limitations and sensitivity of the single technique. Less frequently, SR X-ray analyses are combined with SR micro-photoluminescence or micro-Fourier Transform Infrared spectroscopy, which provide complementary information on the molecular composition, offering a unique integrated analysis approach. Although the spatial correlation between the maps obtained with different techniques is not straightforward due to the different volumes probed by each method, the combination of the information provides a greater understanding and insight into the paint chemistry. In this work, we discuss the advantages and disadvantages of the combination of X-ray techniques and SR-based photoluminescence through the study of two paint micro-samples taken from Pablo Picasso's *Femme* (1907). The painting contains two cadmium yellow paints (based on CdS): one relatively intact and one visibly degraded. SR micro-analyses demonstrated that the two Cd-yellow paints differ in terms of structure, chemical composition, and photoluminescence properties. In particular, on the basis of the combination of different SR measurements, we hypothesize that the degraded yellow is based on nanocrystalline CdS with high presence of Cd(OH)Cl. These two characteristics have enhanced the reactivity of the paint and strongly influenced its stability.

**Key words:** cadmium sulfide, cadmium yellow, painting degradation, synchrotron micro-photoluminescence, synchrotron radiation

(Received 23 February 2022; revised 9 May 2022; accepted 19 May 2022)

## Introduction

Recent years have experienced a growing interest in the investigation of cultural heritage materials through the use of synchrotron radiation (SR) based techniques (Cotte et al., 2008, 2010, 2019; Bertrand et al., 2012; Janssens et al., 2013, 2017). Applications involve different types of objects (e.g., paintings, stones, glasses, porcelains, papyri, textiles, plastics, wooden materials, etc.) and different analytical methods (Bertrand et al., 2012; Cotte et al., 2019), that were employed either to identify the constituent materials and the manufacturing processes and/or to assess the conservation state via definition of the degradation pathways (Cotte et al., 2008, 2019; Bertrand et al., 2012; Janssens et al., 2017; Miliani et al., 2018).

\*Corresponding authors: Marta Ghirardello, E-mail: [marta.ghirardello@polimi.it](mailto:marta.ghirardello@polimi.it); Marine Cotte, E-mail: [marine.cotte@esrf.fr](mailto:marine.cotte@esrf.fr)

Cite this article: Ghirardello M et al (2022) Application of Synchrotron Radiation-Based Micro-Analysis on Cadmium Yellows in Pablo Picasso's *Femme*. *Microsc Microanal.* doi:10.1017/S1431927622000873

The strong demand for SR-based techniques is due to their unique instrumental capabilities and source properties, such as brightness, small beam size, broad spectral range (from the infrared to the hard X-ray), and energy tunability (Cotte et al., 2008). These properties have led to the development of a wide range of analytical techniques (Bertrand et al., 2012; Cotte et al., 2019; Gonzalez et al., 2020a) offering structural characterization, high elemental sensitivity, chemical specificity, and three-dimensional imaging with spatial resolution down to the nanometric length scale. These characteristics are particularly beneficial for the study of highly heterogeneous and complex samples from cultural heritage, such as those from paintings (Cotte et al., 2006, 2008; Cartechini et al., 2008; Keune et al., 2015; Otero et al., 2018; Monico et al., 2019; Vanmeert et al., 2019), which in general are composed of micrometric multi-layered systems with different chemical compositions. The high heterogeneity and complexity of such samples can be further increased by the presence of degradation phenomena.

Typically, paint micro-samples are analyzed with a combination of different SR X-ray based techniques to overcome the

intrinsic limitations and sensitivity of the single techniques. Notably, X-ray fluorescence (XRF) is used for elemental analysis and can be complemented with X-ray absorption spectroscopy (XAS) to define the chemical speciation of an element of interest, and with X-ray diffraction (XRD) for crystalline phase identification and quantification (Cotte et al., 2019). In general, elemental, chemical speciation, and crystalline phase maps can be obtained by raster scanning the sample over 2D regions. Less frequently, SR X-ray analyses are combined with other SR-based techniques, such as micro-photoluminescence ( $\mu$ PL) or micro-Fourier Transform Infrared ( $\mu$ FTIR) spectroscopy (Salvadó et al., 2011, 2014; Lluveras-Tenorio et al., 2012; Pouyet et al., 2015; Langlois et al., 2017; Gonzalez et al., 2020b). Such non-X-ray techniques provide complementary information on the molecular composition, offering a unique integrated approach for the analysis of painting materials.

In particular, SR  $\mu$ PL proved to be a powerful tool for characterizing complex cultural heritage materials down to the submicrometric scale, thanks to the sensitivity of PL to small variations of local environment (Thoury et al., 2016; Hageraats et al., 2019; Thoury et al., 2019). For example, recently SR  $\mu$ PL studies on lead white paint have demonstrated that the spectral unfolding of the PL emission can be used to perform semi-quantitative characterization of the spatial distribution of different lead white crystalline phases in paint layers, without exposing samples to a high dose of ionizing radiation, as could be the case when using synchrotron X-ray beams (Gonzalez et al., 2020b). A major limitation of PL remains the difficulty in interpreting the luminescence spectrum and associating the emission with a specific compound. Indeed, cultural heritage samples are often composed of many different emitting compounds (such as pigments, varnishes, and binders) resulting in a complex emission spectrum.

In this work, we present the combination of SR  $\mu$ PL and SR X-ray based techniques on a case study of two cadmium-based micro-samples from Pablo Picasso's painting *Femme* (1907, Foundation Beyeler, Riehen/Basel, Switzerland) (Comelli et al., 2019). The painting contains two different types of cadmium yellow (CdY) paints which, although exposed to the same

environmental conditions, present different conservation states. While one yellow area has maintained its bright yellow coloration, the other has become brownish. The properties of the preserved and the altered samples are here compared to evaluate similarities with other case studies (Van Der Snickt et al., 2009, 2012; Mass et al., 2013b; Pouyet et al., 2015; Monico et al., 2020a) and to determine potential markers linked to cadmium yellow degradation. The complementarity of SR X-ray based and SR  $\mu$ PL measurements, applied for the first time to the study of the luminescent emission of CdS in degraded CdY paints, are evaluated and the pros and cons of the combined approach are discussed.

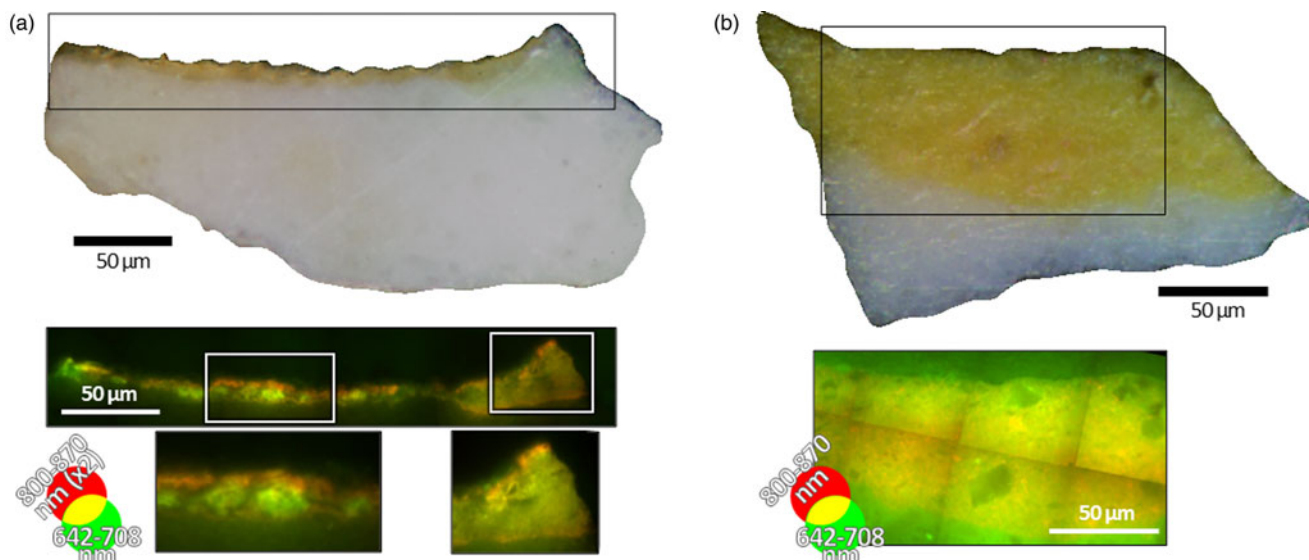
## Materials and Methods

### Samples Description

Two paint micro-samples, selected from representative areas of the degraded yellow (defined as “now-brownish yellow”) and well-preserved yellow (hereafter referred to as “vibrant yellow”) paints of Picasso's *Femme*, were embedded in resin (Technovit LC2000) and prepared for the analysis in cross-section. The resin blocks were resized to the minimum thickness [block size  $\sim 5 \times 4 \times 1 \text{ mm}^3$  ( $l \times w \times h$ )], to reduce the X-ray absorption by the resin. Results of the preliminary characterization, reported in Comelli et al. (2019), are summarized in Supplementary Table S1. Both samples are composed of two layers (Figs. 1a, 1b) and consist of a lead white ground and a Cd-based yellow paint.

### Methods

The irradiation by SR-based X-ray micro-probes of fragile historical materials might itself induce molecular changes in these objects (Bertrand et al., 2015; Monico et al., 2020b). The extent of X-ray damage depends either on the material itself (chemical composition) or on the working conditions (fluence/dose, air/vacuum, and ambient/cryogenic temperature). Such changes may result in the darkening of the sample's surface, obscuring the



**Fig. 1.** Visible light and false-color image of the PL emission (obtained with 275 nm excitation) of the two micro-samples belonging to the (a) now-brownish and (b) vibrant yellow. False-color images of the PL emission are obtained by combining images in the bands 642–708 nm (green) and 800–870 nm (red). Images are recorded as mosaic of different tiles, visible in panel (b). In now-brownish sample, the red channel has been multiplied by a factor 2 for a better visibility.

optical PL emission associated with the original material. To overcome this issue, it is mandatory to start systematically with the collection of SR  $\mu$ PL images prior to analysis with X-ray based methods, as performed in this case.

#### Synchrotron Deep-UV Excited $\mu$ PL at SOLEIL

The two micro-samples were analyzed at the TELEMOS microimaging end-station of the DISCO beamline at the SOLEIL synchrotron (Saint-Aubin, Gif-sur-Yvette, France). The TELEMOS end-station, described in Thoury et al. (2011b), is based on a full-field, fully automatized inverted microscope equipped with a dichroic mirror with a cut-off at 300 nm. The excitation wavelength was varied to 250, 275, and 290 nm and photoluminescence micro-images were recorded with a 100 $\times$ /1.25 NA Zeiss Ultrafluor objective using seven emission filters and variable exposure times to maximize the signal and dynamic range while avoiding saturation. Filters cover the spectral ranges between 420–480 nm, 499–529 nm, 535–607 nm, 642–708 nm, 698–766 nm, and 800–870 nm. A region of interest was defined on each cross section and recorded as a mosaic consisting of different tiles. The images recorded in the different spectral bands were corrected for detector efficiency, filter spectral efficiency, and exposure time and then normalized to the emission peak. False color images of the emission are created by employing the Fiji software (Schindelin et al., 2012) assigning images of interest to red (R) and green (G) channels.

#### Synchrotron $\mu$ XRF and $\mu$ XANES at ESRF-EBS

High lateral resolution information on the distribution and speciation of Cd, Cl, and S was obtained by performing 2D  $\mu$ XRF mapping and fluorescence mode X-ray absorption near-edge structure ( $\mu$ XANES) spectroscopy analysis at S K-, Cl K-, and Cd L<sub>3</sub>-edges at the scanning X-ray microscope (SXM) end-station hosted at the beamline ID21 (Cotte et al., 2017), benefiting from the recently commissioned “Extremely Bright Source” of the European Synchrotron, ESRF-EBS (Grenoble, France). Investigations were carried out using the new double crystal Si(111) monochromator developed by the ESRF (Baker et al., 2018), delivering a highly stable beam in both static and dynamic modes. The beam was kept stable within the beam size while scanning the energy across the S K-, Cl K-, and Cd L<sub>3</sub>-edges, but also while switching from one edge to another. This is an asset for multi-edge XANES analyses such as those conducted in this study, since it allows the speciation of various elements without losing time for beamline realignment. The energy calibration was performed using reference powders of CaSO<sub>4</sub>·2H<sub>2</sub>O, NaCl, and a metallic Cd foil.

The incident beam was focused with Kirkpatrick-Baez mirrors down to a square beam of 0.36  $\times$  0.33  $\mu$ m<sup>2</sup> ( $h \times v$ ), benefiting from the reduced horizontal emittance achieved with EBS (decreased from 4 nm to 110 pm). XRF signals were collected in the horizontal plane and at 69° with respect to the incident beam direction with a 100 mm<sup>2</sup> Sirius Series SDD (Silicon Drift Detector) detector (SGX Sorterch), and Falcon X readout electronics (Xia LLC).

$\mu$ XRF maps were recorded by employing a monochromatic primary beam of fixed energy either at 3.65 or 7.2 keV and with a dwell time of 50 ms/pixel. The software PyMca was used to fit the XRF spectra and to separate the contribution of different elements (Solé et al., 2007).

Single-point fluorescence mode  $\mu$ XANES spectra were acquired by scanning the primary energy across the absorption edges of S, Cl, and Cd, according to the following parameters: S K-edge

(2.46–2.53 keV; energy step: 0.15 eV), Cl K-edge (2.81–2.89 keV; energy step: 0.25 eV), and Cd L<sub>3</sub>-edge (3.52–3.65 keV; energy step: 0.32 eV). Data processing of single-point  $\mu$ XANES spectra was performed with the ATHENA software (Ravel & Newville, 2005). Spectra were normalized and fitted with a linear combination fit (LCF) of library XANES spectra of S- and Cd-based reference compounds. The LCF procedure allowed the quantitative determination of the relative amount (percentage) of sulfate (S<sup>VI</sup>), sulfite (S<sup>IV</sup>), and sulfide (S<sup>II</sup>) species (expressed as %[S<sup>VI</sup>]/[S<sub>total</sub>], %[S<sup>IV</sup>]/[S<sub>total</sub>], and %[S<sup>II</sup>]/[S<sub>total</sub>]) and of different Cd compounds.

#### Synchrotron $\mu$ XRD at ESRF-EBS

2D  $\mu$ XRD maps were recorded on the same cross-sections at the “micro-branch” end-station of beamline ID13 at ESRF (Riekkel et al., 2010), benefitting from the Historical Materials “Block Allocation Group” (BAG) access (Cotte et al., 2022). The incident energy (13 keV) was selected by means of a Si(111) crystal monochromator, while compound refractive lenses (CRL) —mounted in a translocator— were employed to focus the beam down to 2.5  $\times$  2.5  $\mu$ m<sup>2</sup> ( $h \times v$ ). XRD signals were recorded in transmission geometry using a Dectris EIGER X 4M detector (2,070  $\times$  2,167 pixels, pixel size 75  $\times$  75  $\mu$ m<sup>2</sup>) with an acquisition time of 25 ms/pixel. Calibration of the setup was performed using an Al<sub>2</sub>O<sub>3</sub> reference sample. The recorded 2D diffraction images were azimuthally integrated using the Jupyter Notebooks based on the PyFAI software package (Ashiotis et al., 2015) and subsequently analyzed using the XRDU software package (De Nolf et al., 2014).

## Results

#### Synchrotron Deep-UV Excited $\mu$ PL at SOLEIL

Figure 1 shows the false-color image of the SR  $\mu$ PL emission for each sample, obtained by combining the images at 642–708 nm (green channel) and 800–870 nm (red channel), excited with deep-UV light at 275 nm. Similar results were found with other excitation wavelengths (data not reported).

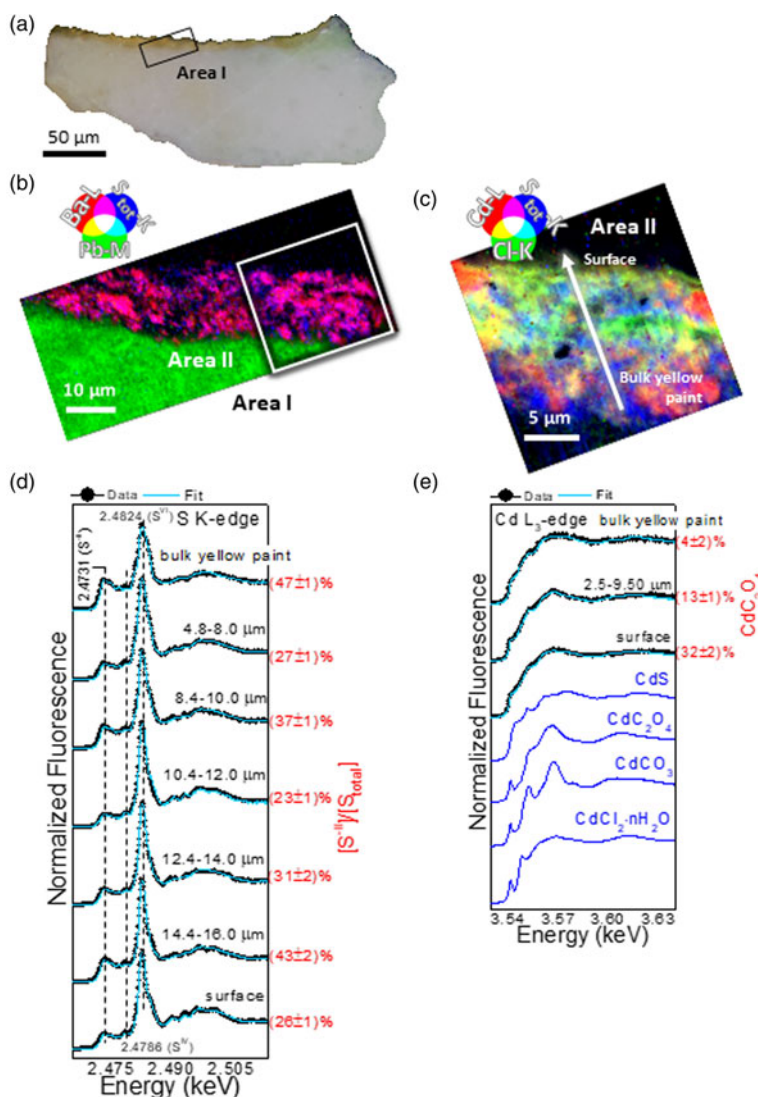
The use of SR  $\mu$ PL imaging allows to observe a high spatial heterogeneity of the optical emission in the altered CdS paint films (Fig. 1a), with regions at the top and at the bottom of the CdY paint layer emitting weakly in the NIR (800–870 nm) and an intermediate region that brightly fluoresces in the red (642–708 nm). Interestingly, this heterogeneity is measured only in the now-brownish yellow paint, while vibrant yellow presents a more homogeneous emission within the whole yellow paint layer (Fig. 1b) peaked in the 800–870 nm spectral range. The emission at shorter wavelengths can be related to the emission of the binding medium (peaked at 535–607 nm) (see Supplementary Fig. S1).

The vibrant yellow paint is characterized by a NIR emission (800–870 nm), typical of CdS deep trap states (Thoury et al., 2011a; Cesaratto et al., 2014; Rosi et al., 2016). This emission, due to defects in the crystal structure of CdS (Thoury et al., 2011a; Giacometti et al., 2018), is highly favored in CdS-based pigment with respect to other emissions, such as the near-band-edge radiative recombination (Cesaratto et al., 2014; Ghirardello et al., 2020a). The emission of the degraded yellow paint, instead, is more intense in the band 642–708 nm, occurring at shorter wavelengths than would be expected for the common deep trap state emission of Cd-based paints (Rosi et al., 2016).

### SR $\mu$ XRF, $\mu$ XANES, and $\mu$ XRD at ESRF-EBS

The elemental composition of the two yellows, detected through SR  $\mu$ XRF, shows that the now-brownish yellow layer is mainly composed of Cd, S, and Ba, while Pb is dominant in the white ground layer (Fig. 2b and Supplementary Fig. S3b). The widespread presence of Cl was also revealed in the now-brownish yellow paint layer, spatially co-localized with the distribution of Cd (Fig. 2c and Supplementary Fig. S3c) though pockets of Cd without Cl are also apparent. The vibrant yellow paint contains the same elements found in the now-brownish sample (Cd, S, Ba, and Pb), although Pb is present in both the yellow and the white layers (see Supplementary Fig. S4). In this case, chlorine is distributed only at the surface of the paint as a very thin layer (with a thickness less than  $3\ \mu\text{m}$ ) with less correlation with the distribution of Cd (Fig. 3b).

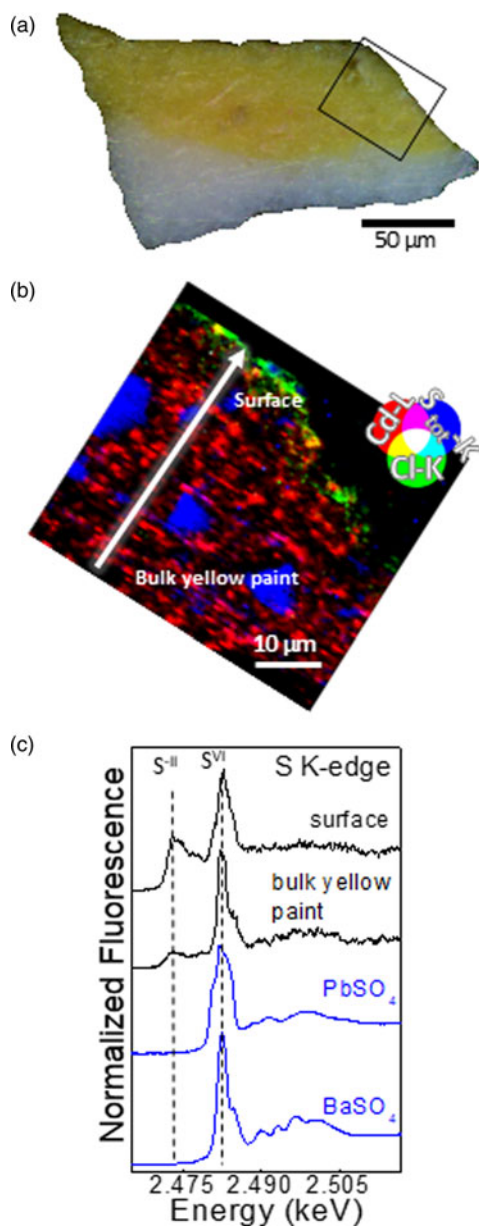
To determine the nature and distribution of the various Cd, S, and Cl species through the stratigraphy of the yellow paint layer, a series of  $\mu$ XANES line spectra at the S K-, Cl K-, and Cd L<sub>3</sub>-edges were acquired at different depths below the paint surface, extending down into the ground layer for both cross-sections. XANES spectra of S- and Cd-based reference compounds are reported in Figures 2e, 3c and Supplementary Figure S2. The series of S K-edge  $\mu$ XANES spectra (Figs. 2d, 3c and Supplementary Fig. S3d and Table S2) highlights, besides CdS (peak at 2.4731 keV), the presence of sulfate species (white line at 2.4824 keV) in both yellows. The method which consists in acquiring the same  $\mu$ XRF map at two energies (the sulfides and sulfates white line energies) (Van Der Snickt et al., 2009; Monico et al., 2018) to map the relative amount of Cd-sulfate ( $\text{S}^{\text{VI}}$ ) versus Cd-sulfide ( $\text{S}^{\text{-II}}$ ) cannot be applied here due to the presence of other sulfate species



**Fig. 2.** Now-brownish yellow sample. (a) Visible light microscopy image of the cross section. RGB composite SR  $\mu$ XRF maps of (b) Ba/Pb/S and (c) Cd/Cl/S [step size ( $h \times v$ ),  $0.25 \times 0.25\ \mu\text{m}^2$ ; exp. time, 50 ms/pixel; energy area I: 7.2 keV; energy area II: 3.65 keV]. In (a,b), the black and white rectangles correspond to the regions where SR  $\mu$ XRF analysis of panels (b,c) were performed. (d,e) Series of  $\mu$ XANES spectra (black) recorded at (d) S K-edge and (e) Cd L<sub>3</sub>-edge and linear combination (LCF) results (cyan) of different S-/Cd-based reference compounds (for details, see Supplementary Tables S2 and S3). In blue, spectral profiles of selected reference compounds (see also Supplementary Fig. S2). In (d,e), spectra were recorded across the line shown in (c) with steps of  $0.4\text{--}0.5\ \mu\text{m}$  and averaged within the depth values reported in each panel (for further data, see Supplementary Fig. S3).

( $\text{PbSO}_4$ ,  $\text{BaSO}_4$ ). However, the identification and localization of these sulfate species were achieved with  $\mu\text{XRD}$  (as explained below).

By fitting S K-edge  $\mu\text{XANES}$  spectra as linear combinations of reference spectra, some conclusions can be drawn with respect to the distribution of the different  $\text{S}^{\text{VI}}$ -compounds within the yellow layers (see Supplementary Table S2). In the now-brownish yellow,  $\text{PbSO}_4$  is the dominant component along with minor amounts of  $\text{CdSO}_4/\text{CdSO}_4 \cdot \text{H}_2\text{O}$  in the bottommost  $10 \mu\text{m}$  of the sample, whereas  $\text{BaSO}_4$  and  $\text{CdSO}_4/\text{CdSO}_4 \cdot \text{H}_2\text{O}$  are the main compounds of the uppermost surface of the paint. In addition to sulfides and sulfates, S K-edge  $\mu\text{XANES}$  spectra show the additional presence of sulfites ( $\text{S}^{\text{IV}}$ ; signal at  $2.4786 \text{ keV}$ ), as reported in other case



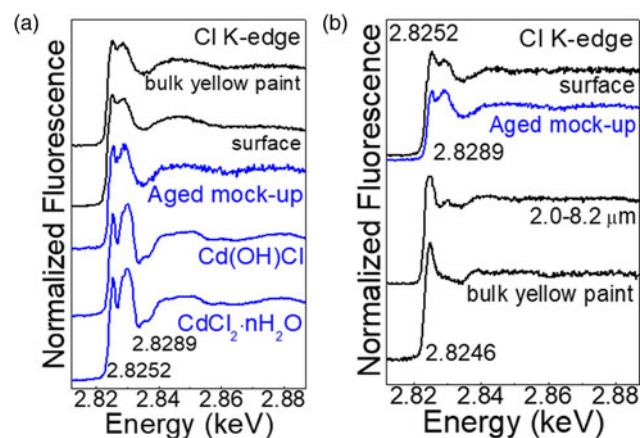
**Fig. 3.** Vibrant yellow sample. (a) Visible light microscopy image of the cross section. Area marked in black corresponds to the SR  $\mu\text{XRF}$  map of panel (b). (b) RGB composite SR  $\mu\text{XRF}$  maps of Cd/Cl/S [step size ( $h \times v$ ),  $0.5 \times 0.5 \mu\text{m}^2$ ; exposure time, 50 ms/pixel; energy, 3.65 keV]. (c) Selection of  $\mu\text{XANES}$  spectra (black) recorded at S K-edge from the line shown in (b) compared to those of reference compounds.

studies of degraded CdS (Monico et al., 2018; Monico et al., 2020a). Notably, sulfite species are related to intermediate mechanisms of the oxidation of sulfides to sulfates (Monico et al., 2020a). In the vibrant yellow paint, LCF of S K-edge XANES spectra was not performed, since the contribution of the Pb  $M_5$  XRF emission line strongly overlaps with S K-lines. Spectral features characteristic of  $\text{PbSO}_4$  were apparent at the paint surface, with other  $\text{S}^{\text{IV}}$ -species.

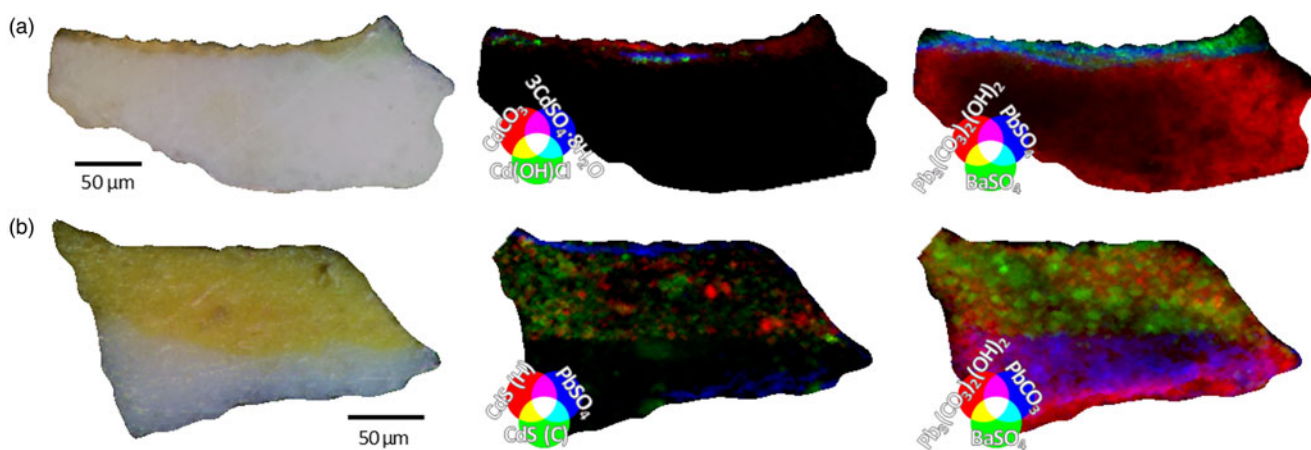
Results of the LCF on Cd  $L_3$ -edge XANES line scans show the presence of CdS in both samples (see Supplementary Table S3). However, while in the vibrant yellow CdS is the dominant chemical component (data not shown), the now-brownish yellow paint shows an enrichment of Cd-Cl compounds and  $\text{CdC}_2\text{O}_4$ , the latter mainly located at the paint surface (Fig. 2e and Supplementary Fig. S3e and Table S3).

The  $\mu\text{XANES}$  line scans at the Cl K-edge in the now-brownish yellow show similar spectra throughout the entire layer (Fig. 4a). Spectral features show a good agreement with those of profiles previously recorded on artificially aged paint mock-ups originally containing cadmium hydrochloride ( $\text{Cd}(\text{OH})\text{Cl}$ ) (Monico et al., 2020a) and amorphous Cd-Cl compounds. In the vibrant yellow, instead, only the spectra recorded within the uppermost few micrometres of the paint surface show features that resemble an amorphous Cd-Cl compound (Fig. 4b). The profiles recorded in the bulk of the paint do not appear to match with Cd-Cl compounds. While their assignment remains uncertain, the spectral features are similar to those of oxychlorinated- and/or organochlorinated-compounds (Vaudey et al., 2011; Leri et al., 2015).

SR  $\mu\text{XRD}$  2D maps provided information on the nature and distribution of the different constituent crystalline phases in the two samples. The now-brownish yellow paint (Fig. 5a) is composed of  $\text{BaSO}_4$ , cadmium carbonate ( $\text{CdCO}_3$ ), 8/3-hydrate cadmium sulfate ( $3\text{CdSO}_4 \cdot 8\text{H}_2\text{O}$ ), and  $\text{PbSO}_4$ , this latter mainly concentrated at the interface between the yellow CdS and the lead white ground. Cd(OH)Cl is also detected in the now-brownish yellow layer, spatially localized in a similar region of  $3\text{CdSO}_4 \cdot 8\text{H}_2\text{O}$ , in agreement with previous research (Monico et al., 2020a). Interestingly, although the presence of CdS has been detected in the now-brownish layer through XANES, neither hexagonal nor cubic CdS are detected by  $\mu\text{XRD}$ . This suggests that the pigment is likely amorphous or nanocrystalline. The vibrant yellow (Fig. 5b) is mainly composed of hydrocerussite



**Fig. 4.** Series of Cl K-edge  $\mu\text{XANES}$  spectra (black) recorded from (a) now-brownish yellow and (b) vibrant yellow. In blue, spectral profiles of selected Cl reference compounds. Spectra were recorded across the lines shown in Figures 2c and 3b with steps of  $0.4\text{--}0.5 \mu\text{m}$  and averaged within the depth values reported in each panel.



**Fig. 5.** SR  $\mu$ XRD distribution in (a) now-brownish yellow and (b) vibrant yellow of the different crystalline phases identified [step size ( $h \times v$ ),  $1 \times 1 \mu\text{m}^2$ ; exposure time, 25 ms/pixel; energy, 13 keV]. The darker region in the center of the maps is due to the poor transparency of the sample (mainly composed of Pb) to X-ray (measurements were acquired in transmission mode).

[ $\text{Pb}_3(\text{CO}_3)_2(\text{OH})_2$ ],  $\text{BaSO}_4$ , and sparse grains of CdS in both crystalline forms (hexagonal and cubic).  $\text{PbSO}_4$  is also detected in the yellow layer and is spatially localized in an area corresponding to the surface of the painting. The white ground, common to both samples, is composed of cerussite ( $\text{PbCO}_3$ ) and hydrocerussite.

## Discussion

### Combination of Different SR-Based Techniques

The spatial correlation between the maps obtained with different SR techniques is challenging due to the different volumes probed by each method. Although providing an accurate estimate of the probing depth of DUV and X-ray excitation is rather difficult due to the dependence on multiple parameters (such as material properties, layer thickness, excitation energy, and reabsorption effects), the penetration depth of DUV light excitation (tens of nanometres to few microns, depending on the material) reduced the probed volume compared to that examined with X-ray analyses (few microns for XANES at 2.5–3.5 keV and tens of microns for XRD at 13 keV). Consequently, PL images are related to the signal from the exposed surface of the cross-section, while X-ray information is related to a larger volume for XANES and to the entire cross-section for XRD. Data interpretation is further complicated by the fact that the sensitivity of each technique depends on materials composition and properties.

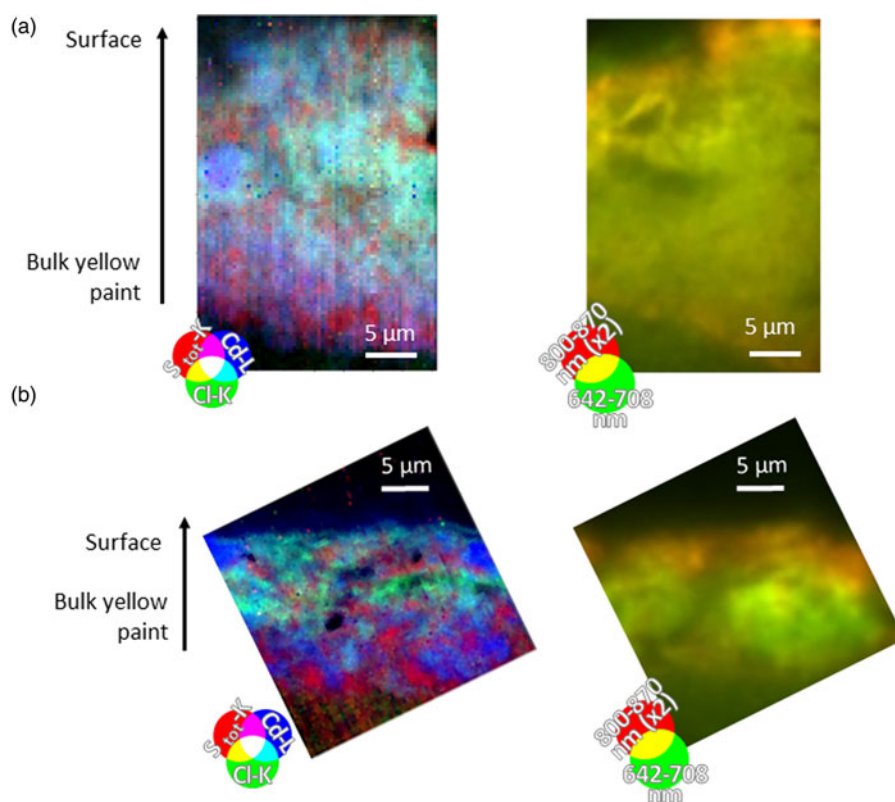
Considering these issues, it is clear that the superimposition of distributional maps from different techniques is not straightforward. Nonetheless, the combination of the molecular information provided by each technique allows us to achieve a clearer characterization of the samples and to provide a clearer comprehension of  $\mu$ PL data.

Focusing on the now-brownish yellow, we can infer the following observations:

- (i) Upon deep-UV excitation, the paint exhibits an intense optical emission. Among the compounds identified through  $\mu$ XRD and  $\mu$ XANES, the only one that is well-known for its optical emission is CdS (Gaft et al., 2015; Comelli et al., 2019), while all the other identified compounds are low- or non-emitting materials. Hence, the optical emission of the degraded CdY paint has to be ascribed to CdS and, in

particular, to the radiative emission occurring from deep trap states induced by defects. Indeed, the emission occurs at longer wavelengths than the near-band-edge emission of CdS (Thoury et al., 2011a; Cesaratto et al., 2014; Rosi et al., 2016).

- (ii)  $\mu$ XRD and  $\mu$ XANES infer the presence of CdS as an amorphous or nanocrystalline material. While amorphous CdS should present a faint optical emission, highly defective CdS nanoparticles in general present an intense emission from trap states (Veamatahau et al., 2015). Therefore, we can hypothesize that the pigment is based on nanocrystalline CdS, as has been already identified in other degraded cadmium yellow paints (Levin et al., 2019). The large surface-to-volume ratio of CdS nanoparticles causes them to easily react with the surrounding environment, giving them a low stability and high reactivity (Xu et al., 2018) thus contributing to paint degradation.
- (iii) *In-situ* measurements (Comelli et al., 2019) on the now-brownish yellow paint have shown only the presence of an intense emission peaked at 650 nm. SR  $\mu$ PL analysis allowed a more complex situation to be defined, with the presence of NIR emission in the uppermost and bottommost part of the yellow layer and red emission in the innermost part. Interestingly,  $\mu$ XRF and  $\mu$ PL maps display a certain degree of correlation, both displaying different signals at the surface and at the bottom of the degraded paint with respect to its inner part. In details, the comparison of the elemental distribution achieved through  $\mu$ XRF maps and the PL emission shows that Cd-rich areas (without Cl, blue areas in RGB composite of  $\mu$ XRF maps in Fig. 6) present NIR PL emission (800–870 nm). Instead, areas containing Cd and Cl (cyan in RGB composite of  $\mu$ XRF maps in Fig. 6) are more correlated with the emission occurring in the band 642–708 nm (green in false RGB PL images in Fig. 6). Based on this correlation, we hypothesize that chlorine species affected the paint micro-environment and consequently the stability of the highly reactive poorly crystalline CdS, inducing the formation of a high-density of superficial defects (Lee et al., 2012) that are responsible of the intense PL emission observed. To confirm this hypothesis, further artificial ageing test on paint models with measurements before and after degradation are necessary.



**Fig. 6.** Comparison between SR  $\mu$ XRF maps and false-color image of the PL emission of two different region of the now-brownish sample. Panel (a) shows part of the region of interest reported in Supplementary Figure S3, panel (b) the region of interest reported in Figure 2b. The RGB composite of SR  $\mu$ XRF maps of Cd/S/Cl [step size ( $h \times v$ ),  $0.25 \times 0.25 \mu\text{m}^2$ ; exp. time, 50 ms/pixel; energy, 3.65 keV] and the corresponding false-color image of the PL emission [275 nm excitation, green = 642–708 nm, red = 800–870 nm (multiplied by a factor 2)] are reported for each region.

### Comparison with Previous Case Studies

X-ray-based analysis revealed that Picasso employed (at least) two different CdY paints in the painting. The vibrant yellow is mainly composed of a mixture of crystalline hexagonal and cubic CdS with two different extenders [ $\text{Pb}_3(\text{CO}_3)_2(\text{OH})_2$  and  $\text{BaSO}_4$ ], while the now-brownish yellow is made up of a mixture of amorphous or nanocrystalline CdS and  $\text{BaSO}_4$ . This finding provides the first clear evidence of the different crystallinity of CdS in the two yellow paints belonging to Picasso's *Femme*.

Cl compounds are present in both vibrant and now-brownish paints. In the vibrant yellow sample, amorphous Cd–Cl species are limited to the surface of the paint layer, while the bulk shows Cl compounds with an unidentified chemical speciation and in an extremely low amount. Instead, in the now-brownish paint, the Cl species could be identified as  $\text{Cd}(\text{OH})\text{Cl}$  and amorphous Cd–Cl compounds, and were found widespread throughout the paint stratigraphy.

The poor crystallinity of the now-brownish yellow and the presence of  $\text{Cd}(\text{OH})\text{Cl}$  can be ascribed to the production method of the pigment, in particular to wet synthesis processes that produced a poorly crystalline pigment with an abundance of synthesis residues (Leone et al., 2005; Mass et al., 2013a; Levin et al., 2019; Ghirardello et al., 2020b). In previous work (Ghirardello et al., 2020b), we have detected chlorine contaminations only in pigments synthesized from  $\text{CdCl}_2$ . Therefore, it is reasonable to ascribe the presence of Cl to the synthesis method. Moreover, the identification of cadmium carbonate in the now-brownish paint further supports the hypothesis that a specific wet synthesis

method [the indirect wet process (Mass et al., 2013b; Pouyet et al., 2015; Levin et al., 2019)] could have been employed for the CdS pigment found in the altered yellow area.

Although the two paints have been exposed to the same environmental conditions, the different types of CdS pigment along with some residual of the starting reagents (i.e., chlorine species) have influenced the paint stability, leading to degradation where a poorly crystalline CdY pigment was used, accompanied by residual contamination from the synthesis process. This finding on the specific case study of *Femme* is in agreement with other publications on other degraded cadmium yellow paints (Leone et al., 2005; Pouyet et al., 2015; Monico et al., 2020a), that have similarly shown the presence of poorly crystalline or nanocrystalline (Levin et al., 2019) CdS pigments, together with the presence of chlorine compounds. The occurrence of these two features on an increasing number of historical degraded paintings confirm their key role in CdY paint degradation and paves the way for future work on artificially aged model paints focusing on clarifying the individual role of these two factors.

$\text{PbSO}_4$  was detected in both samples. Based on previous studies, this compound can be associated with the degradation of lead white (Gonzalez et al., 2020c). In paintings with both CdY and lead white, the development of  $\text{PbSO}_4$  was linked with the oxidation of CdS and to the formation of the more stable salt than  $\text{CdSO}_4$  ( $\text{PbSO}_4$ ) (Van Der Snickt et al., 2012), although it is noted that  $\text{PbSO}_4$  can also form as a consequence of the reaction of lead white with environmental  $\text{SO}_2$  (Szlachetko et al., 2010; Price et al., 2019).  $\text{PbSO}_4$  is present in both paints but to different extents. In the now-brownish yellow,  $\text{PbSO}_4$  is present mainly and



with higher concentration (see Supplementary Table S2) at the interface between the yellow and the white ground. Since the lower white ground layer is shielded from the environment by the yellow paint layer above, the presence of  $\text{PbSO}_4$  at this interface could be reasonably linked to the reaction within the paint layers (Van Der Snickt et al., 2009). In the vibrant yellow,  $\text{PbSO}_4$  has formed as a thin layer on the sample surface only, suggesting that its formation is likely the consequence of the interaction with the environment.

In addition to the different CdYs used, it is also interesting to note that two different sub-types of lead white pigment were used in the painting. The white used for the ground contains the usual two constitutive phases of lead white, cerussite and hydrocerussite. However, the one mixed with the vibrant yellow paint contains only hydrocerussite. The painting (dated 1907) was created in a key moment for the production of lead white: indeed, the historical synthesis of lead white based on lead corrosion was still in use alongside new production routes based on precipitation (Gonzalez et al., 2019, 2016, 2017). A lead white paint entirely composed of hydrocerussite (as the one mixed with CdS in vibrant yellow) is difficult to obtain following the historical lead white synthesis (Gonzalez et al., 2019), and might thus correspond to the use of a modern synthesis process. In contrast, the white ground with its mixed composition of hydrocerussite and cerussite is linked to the traditional synthesis process.

### Conclusion and Future Perspective

The results obtained from SR measurements, exploiting the improved performances of ESRF-EBS (Cotte et al., 2019), refurbished ID21 and the combination with SR  $\mu\text{PL}$  allowed us to observe new chemical and structural features in both samples [e.g., different CdS crystallinity, presence of  $\text{Cd}(\text{OH})\text{Cl}$  and clear identification of degradation species]. Although the correlation of the distribution maps is not straightforward, the combination of the information provided by the different techniques demonstrated to be fundamental to achieve a better understanding of the samples.

The experience gained by the application of this SR-based multi-analytical protocol states that the main difficulties in data integration is caused by the differences in the volumes probed by the different measurement modalities. In this framework, the use of thin sections ( $\sim 10\ \mu\text{m}$ ) allows to probe a similar sample volume (at least for XANES and XRD), while also increasing the homogeneity of the sample along the radiation direction. Moreover, to achieve a better correlation with X-ray-based analysis, the X-ray excited optical luminescence could also be employed (Hageraats et al., 2021).

Focusing on the specific study of the degradation of cadmium yellow paints, in the close future the study of less complex artificially aged model samples with a combination of SR X-ray and PL techniques will allow us to achieve a further step in the comprehension of the factors triggering the stability of this paint. CdY paints prepared *ad hoc* from different historically reconstructed pigments will be systematically studied with a combination of  $\mu\text{XRF}$ ,  $\mu\text{XANES}$ ,  $\mu\text{XRD}$ , and  $\mu\text{PL}$  measurements to understand the role of particle size and chlorine compounds on the stability of CdY oil paints.

**Supplementary material.** To view supplementary material for this article, please visit <https://doi.org/10.1017/S1431927622000873>.

**Acknowledgments.** The authors wish to thank Markus Gross and Fondation Beyeler (Riehen/Basel, Switzerland) for providing the samples from *Femme* and allowing their study and colleagues from the Getty Conservation Institute Alan Phenix, Herant Khanjian, Karen Trentelman. This research was carried out at DISCO beamline at SOLEIL (proposal n. 20190111) and at ID21 and ID13 beamlines at ESRF-EBS (proposal HG-159 and in-house beamtime). The proposal HG-159 is a pilot of the Heritage BAG project (proposal HG-172) supported by the European Union's Horizon 2020 research and innovation programme under grant agreement No 870313, Streamline. We thank Loïc Huder and PaNOSC (project funded by the European Union's Horizon 2020 Research and Innovation programme under Grant Agreement No 823852), for data analysis tools (Jupyter notebooks). We thank ESRF accelerator and source division, the ID21 and ESRF instrumentation service and development division colleagues for their efforts in instrumental developments for EBS and ID21 refurbishment, especially Stuart Fisher for the development of *Daiquiri* interface. Financial support by the Access to Research Infrastructures activity in the Horizon 2020 Programme of the EU (IPERION CH Grant Agreement n. 654028) is gratefully acknowledged for SOLEIL measurements.

**Conflict of interest.** The authors declare no competing interests.

### References

- Ashiotis G, Deschildre A, Nawaz Z, Wright JP, Karkoulis D, Picca FE & Kieffer J (2015). The fast azimuthal integration python library: PyFAI. *J Appl Crystallogr* **48**, 510–519.
- Baker R, Baboulin D, Barrett R, Bernard P, Berruyer G, Bonnefoy J, Brendike M, Brumund P, Dabin Y, Ducotté L, Gonzalez H, Malandrino G, Marion P, Mathon O, Roth T & Tucoulou R (2018). ESRF double crystal monochromator prototype project. In *Mechanical Eng. Design of Synchrotron Radiation Equipment and Instrumentation MEDSI2018*, Paris, France.
- Bertrand L, Robinet L, Thoury M, Janssens K, Cohen SX & Schöder S (2012). Cultural heritage and archaeology materials studied by synchrotron spectroscopy and imaging. *Appl Phys A Mater Sci Process* **106**, 377–396.
- Bertrand L, Schöder S, Anglos D, Breese MBH, Janssens K, Moini M & Simon A (2015). Mitigation strategies for radiation damage in the analysis of ancient materials. *TrAC – Trends Analyt Chem* **66**, 128–145.
- Cartechini L, Miliani C, Brunetti BG, Sgamellotti A, Altavilla C, Ciliberto E & D'Acapito F (2008). X-ray absorption investigations of copper resinate blackening in a XV century Italian painting. *Appl Phys A Mater Sci Process* **92**, 243–250.
- Cesaratto A, D'Andrea C, Nevin A, Valentini G, Tassone F, Alberti R, Frizzi T & Comelli D (2014). Analysis of cadmium-based pigments with time-resolved photoluminescence. *Anal Methods* **6**, 130–138.
- Comelli D, MacLennan D, Ghirardello M, Phenix A, Schmidt Patterson C, Khanjian H, Gross M, Valentini G, Trentelman K & Nevin A (2019). Degradation of cadmium yellow paint: New evidence from photoluminescence studies of trap states in Picasso's *Femme* (époque des "demoiselles d'Avignon"). *Anal Chem* **91**, 3421–3428.
- Cotte M, Autran P-O, Berruyer C, Dejoie C, Susini J & Tafforeau P (2019). Cultural and natural heritage at the ESRF: Looking back and to the future. *Synchrotron Radiat News* **32**, 34–40.
- Cotte M, Gonzalez V, Vanmeert F, Monico L, Dejoie C, Burghammer M, Huder L, de Nolf W, Fisher S, Fazlic I, Chauffeton C, Wallez G, Jiménez N, Albert-Tortosa F, Salvadó N, Possenti E, Colombo C, Ghirardello M, Comelli D, Avranovich Clerici E, Vivani R, Romani A, Costantino C, Janssens K, Taniguchi Y, McCarthy J, Reichert H & Susini J (2022). The "historical materials BAG": A new facilitated access to synchrotron X-ray diffraction analyses for cultural heritage materials at the European synchrotron radiation facility. *Molecules* **27**, 1997.
- Cotte M, Pouyet E, Salomé M, Rivard C, De Nolf W, Castillo-Michel H, Fabris T, Monico L, Janssens K, Wang T, Sciau P, Verger L, Cormier L, Dargaud O, Brun E, Bugnaget D, Fayard B, Hesse B, del Real AEP, Veronesi G, Langlois J, Balcar N, Vandenberghe Y, Kieffer VA, Kieffer J, Barrett R, Cohen C, Cornu C, Baker R, Gagliardini E, Papillon E

- & Susini J (2017). The ID21 X-ray and infrared microscopy beamline at the ESRF: Status and recent applications to artistic materials.
- Cotte M, Susini J, Dik J & Janssens K (2010). Synchrotron-based X-ray absorption spectroscopy for art conservation: Looking back and looking forward. *Acc Chem Res* **43**, 705–714.
- Cotte M, Susini J, Metrich N, Moscato A, Gratzu C, Bertagnini A & Pagano M (2006). Blackening of Pompeian cinnabar paintings: X-ray microspectroscopy analysis. *Anal Chem* **78**, 7484–7492.
- Cotte M, Susini J, Solé VA, Taniguchi Y, Chillida J, Checron E & Walter P (2008). Applications of synchrotron-based micro-imaging techniques to the chemical analysis of ancient paintings. *J Anal At Spectrom* **23**, 820–828.
- De Nolf W, Vanmeert F & Janssens K (2014). XRDUA: crystalline phase distribution maps by two-dimensional scanning and tomographic (micro) X-ray powder diffraction. *J Appl Crystallogr* **47**, 1107–1117. <https://doi.org/10.1107/S1600576714008218>.
- Gaft M, Reisfeld R & Panczer G (2015). *Modern Luminescence Spectroscopy of Minerals and Materials*. Berlin, Heidelberg: Springer. <https://doi.org/10.1007/b137490>.
- Ghirardello M, Kelly NM, Valentini G, Toniolo L & Comelli D (2020a). Photoluminescence excited at variable fluences: A novel approach for studying the emission from crystalline pigments in paints. *Anal Methods* **12**, 4007–4014.
- Ghirardello M, Otero V, Comelli D, Toniolo L, Dellasega D, Nessi L, Cantoni M, Valentini G, Nevin A & Melo MJ (2020b). An investigation into the synthesis of cadmium sulfide pigments for a better understanding of their reactivity in artworks. *Dyes Pigm* **186**, 108998.
- Giacopetti L, Nevin A, Comelli D, Valentini G, Nardelli MB & Satta A (2018). First principles study of the optical emission of cadmium yellow: Role of cadmium vacancies. *AIP Adv* **8**, 1–7.
- Gonzalez V, Calligaro T, Wallez G, Eveno M, Toussaint K & Menu M (2016). Composition and microstructure of the lead white pigment in masters paintings using HR synchrotron XRD. *Microchem J* **125**, 43–49.
- Gonzalez V, Cotte M, Vanmeert F, Nolf W & Janssens K (2020a). X-ray diffraction mapping for cultural heritage science: A review of experimental configurations and applications. *Chem Eur J* **26**, 1703–1719.
- Gonzalez V, Hageraats S, Wallez G, Eveno M, Ravaud E, Réfrégiers M, Thoury M, Menu M & Gourier D (2020b). Microchemical analysis of Leonardo da Vinci's lead white paints reveals knowledge and control over pigment scattering properties. *Sci Rep* **10**, 1–10.
- Gonzalez V, Van Loon A, Wt Price S, Noble P & Keune K (2020c). Synchrotron micro-XRD and micro-XRD-CT reveal newly formed lead-sulfur compounds in old master paintings. *J Anal At Spectrom* **35**, 2267–2273.
- Gonzalez V, Wallez G, Calligaro T, Cotte M, De Nolf W, Eveno M, Ravaud E & Menu M (2017). Synchrotron-based high angle resolution and high lateral resolution X-ray diffraction: Revealing lead white pigment qualities in old masters paintings. *Anal Chem* **89**, 13203–13211.
- Gonzalez V, Wallez G, Calligaro T, Gourier D & Menu M (2019). Synthesizing lead white pigments by lead corrosion: New insights into the ancient manufacturing processes. *Corros Sci* **146**, 10–17.
- Hageraats S, Keune K, Réfrégiers M, Van Loon A, Berrie B & Thoury M (2019). Synchrotron deep-UV photoluminescence imaging for the sub-micrometer analysis of chemically altered zinc white oil paints. *Anal Chem* **91**, 14887–14895.
- Hageraats S, Keune K, Stanescu S, Laurent JM, Fresquet W & Thoury M (2021). Combining X-ray excited optical luminescence and X-ray absorption spectroscopy for correlative imaging on the nanoscale. *J Synchrotron Radiat* **28**, 1858–1864.
- Janssens K, Alfeld M, Van Der Snickt G, De Nolf W, Vanmeert F, Radepon M, Monico L, Dik J, Cotte M, Falkenberg G, Miliani C & Brunetti BG (2013). The use of synchrotron radiation for the characterization of artists' pigments and paintings. *Annu Rev Anal Chem* **6**, 399–425.
- Janssens K, Van der Snickt G, Vanmeert F, Legrand S, Nuyts G, Alfeld M, Monico L, Anaf W, De Nolf W, Vermeulen M, Verbeeck J & De Wael K (2017). Non-invasive and non-destructive examination of artistic pigments, paints, and paintings by means of X-ray methods. In *Analytical Chemistry for Cultural Heritage*. Topics in Current Chemistry Collections, Mazzeo R. (Ed.), vol. 374, pp. 77–128. Cham: Springer. [https://doi.org/10.1007/978-3-319-52804-5\\_3](https://doi.org/10.1007/978-3-319-52804-5_3).
- Keune K, Mass J, Meirer F, Pottasch C, Van Loon A, Hull A, Church J, Pouyet E, Cotte M & Mehta A (2015). Tracking the transformation and transport of arsenic sulfide pigments in paints: Synchrotron-based X-ray micro-analyses. *J Anal At Spectrom* **30**, 813–827.
- Langlois J, Mary G, Bluzat H, Cascio A, Balcar N, Vandenberghe Y & Cotte M (2017). Analysis and conservation of modern modeling materials found in auguste rodin's sculptures. *Stud Conserv* **62**, 247–265.
- Lee W, Kim H, Jung DR, Kim J, Nahm C, Lee J, Kang S, Lee B & Park B (2012). An effective oxidation approach for luminescence enhancement in CdS quantum dots by H<sub>2</sub>O<sub>2</sub>. *Nanoscale Res Lett* **7**, 1–5.
- Leone B, Burnstock A, Jones C, Hallebeek P, Boon JJ & Keune K (2005). The deterioration of cadmium sulphide yellow artists' pigments. In *ICOM Committee for Conservation. Triennial Meeting, 14th, The Hague, Netherlands*, Vol. 2, pp. 803–813.
- Leri AC, Mayer LM, Thornton KR, Northrup PA, Dunigan MR, Ness KJ & Gellis AB (2015). A marine sink for chlorine in natural organic matter. *Nat Geosci* **8**, 620–624.
- Levin BDA, Finnefrock AC, Hull AM, Thomas MG, Nguyen KX, Holtz ME, Plahter U, Grimstad I, Mass JL & Muller DA (2019). Revealing the nanoparticle composition of Edvard Munch's The Scream, and implications for paint alteration in iconic early 20th century artworks. *arXiv:1909.01933*.
- Llaveras-Tenorio A, Andreatti A, Bonaduce I, Boularand S, Cotte M, Roqué J, Colombini MP & Vendrell-Saz M (2012). Mass spectrometric and synchrotron radiation based techniques for the identification and distribution of painting materials in samples from paintings of Josep Maria Sert. *Chem Cent J* **6**, 1–18.
- Mass J, Sedlmair J, Patterson CS, Carson D, Buckley B & Hirschmugl C (2013b). SR-FTIR imaging of the altered cadmium sulfide yellow paints in Henri Matisse's Le Bonheur de vivre (1905–6) – Examination of visually distinct degradation regions. *Analyst* **138**, 6032.
- Mass JL, Opila R, Buckley B, Cotte M, Church J & Mehta A (2013a). The photodegradation of cadmium yellow paints in Henri Matisse's le Bonheur de vivre (1905–1906). *Appl Phys A Mater Sci Process* **111**, 59–68.
- Miliani C, Monico L, Melo MJ, Fantacci S, Angelin EM, Romani A & Janssens K (2018). Photochemistry of artists' dyes and pigments: Towards better understanding and prevention of colour change in works of art. *Angew Chem Int Ed* **57**, 7324–7334.
- Monico L, Cartechini L, Rosi F, Chieli A, Grazia C, de Meyer S, Nuyts G, Vanmeert F, Janssens K, Cotte M, de Nolf W, Falkenberg G, Sandu ICA, Tveit ES, Mass J, de Freitas RP, Romani A & Miliani C (2020a). Probing the chemistry of CdS paints in the scream by in situ non-invasive spectroscopies and synchrotron radiation X-ray techniques. *Sci Adv* **6**, 1–11.
- Monico L, Chieli A, De Meyer S, Cotte M, de Nolf W, Falkenberg G, Janssens K, Romani A & Miliani C (2018). Role of the relative humidity and the Cd/Zn stoichiometry in the photooxidation process of cadmium yellows (CdS/Cd<sub>1-x</sub>Zn<sub>x</sub>S) in oil paintings. *Chem Eur J* **24**, 11584–11593.
- Monico L, Cotte M, Vanmeert F, Amidani L, Janssens K, Nuyts G, Garrovet J, Falkenberg G, Glatzel P, Romani A & Miliani C (2020b). Damages induced by synchrotron radiation-based X-ray microanalysis in chrome yellow paints and related Cr-compounds: Assessment, quantification, and mitigation strategies. *Anal Chem* **92**, 14164–14173.
- Monico L, Sorace L, Cotte M, De Nolf W, Janssens K, Romani A & Miliani C (2019). Disclosing the binding medium effects and the pigment solubility in the (photo)reduction process of chrome yellows (PbCrO<sub>4</sub>/PbCr<sub>1-x</sub>S<sub>x</sub>O<sub>4</sub>). *ACS Omega* **4**, 6607–6619.
- Otero V, Vilarigues M, Carlyle L, Cotte M, De Nolf W & Melo MJ (2018). A little key to oxalate formation in oil paints: Protective patina or chemical reactor? *Photochem Photobiol Sci* **17**, 266–270.
- Pouyet E, Cotte M, Fayard B, Salomé M, Meirer F, Mehta A, Uffelman ES, Hull A, Vanmeert F, Kieffer J, Burghammer M, Janssens K, Sette F & Mass J (2015). 2D X-ray and FTIR micro-analysis of the degradation of cadmium yellow pigment in paintings of Henri Matisse. *Appl Phys A Mater Sci Process* **121**, 967–980.
- Price SWT, Van Loon A, Keune K, Parsons AD, Murray C, Beale AM & Mosselmann JFW (2019). Unravelling the spatial dependency of the complex solid-state chemistry of Pb in a paint micro-sample from Rembrandt's Homer using XRD-CT. *Chem Commun* **55**, 1931–1934.

- Ravel B & Newville M (2005). ATHENA, ARTEMIS, HEPHAESTUS: Data analysis for X-ray absorption spectroscopy using IFEFFIT. *J Synchrotron Radiat* **12**, 537–541.
- Riekel C, Burghammer M & Davies R (2010). Progress in micro- and nano-diffraction at the ESRF ID13 beamline. *IOP Conf Ser: Mater Sci Eng* **14**, 012013.
- Rosi F, Grazia C, Gabrieli F, Romani A, Paolantoni M, Vivani R, Brunetti BG, Colombari P & Miliani C (2016). UV-Vis-NIR and micro Raman spectroscopies for the non destructive identification of  $Cd_{1-x}Zn_xS$  solid solutions in cadmium yellow pigments. *Microchem J* **124**, 856–867.
- Salvadó N, Butí S, Aranda MAG & Pradell T (2014). New insights on blue pigments used in 15th century paintings by synchrotron radiation-based micro-FTIR and XRD. *Anal Methods* **6**, 3610–3621.
- Salvadó N, Butí S, Labrador A, Cinque G, Emerich H & Pradell T (2011). SR-XRD and SR-FTIR study of the alteration of silver foils in medieval paintings. *Anal Bioanal Chem* **399**, 3041–3052.
- Schindelin J, Arganda-Carreras I, Frise E, Kaynig V, Longair M, Pietzsch T, Preibisch S, Rueden C, Saalfeld S, Schmid B, Tinevez J-Y, White DJ, Hartenstein V, Eliceiri K, Tomancak P & Cardona A (2012). Fiji: An open-source platform for biological-image analysis. *Nat Methods* **9**, 676–682.
- Solé VA, Papillon E, Cotte M, Walter P & Susini J (2007). A multiplatform code for the analysis of energy-dispersive X-ray fluorescence spectra. *Spectrochim Acta B At Spectrosc* **62**, 63–68.
- Szlachetko J, Cotte M, Morse J, Salomé M, Jagodzinski P, Dousse JC, Hoszowska J, Kayser Y & Susini J (2010). Wavelength-dispersive spectrometer for X-ray microfluorescence analysis at the X-ray microscopy beamline ID21 (ESRF). *J Synchrotron Radiat* **17**, 400–408.
- Thoury M, Delaney JK, De La Rie ER, Palmer M, Morales K & Krueger J (2011a). Near-infrared luminescence of cadmium pigments: In situ identification and mapping in paintings. *Appl Spectrosc* **65**, 939–951.
- Thoury M, Echard JP, Réfrégiers M, Berrie B, Nevin A, Jamme F & Bertrand L (2011b). Synchrotron UV-visible multispectral luminescence microimaging of historical samples. *Anal Chem* **83**, 1737–1745.
- Thoury M, Mille B, Séverin-Fabiani T, Robbiola L, Réfrégiers M, Jarrige JF & Bertrand L (2016). High spatial dynamics-photoluminescence imaging reveals the metallurgy of the earliest lost-wax cast object. *Nat Commun* **7**, 1–8.
- Thoury M, Van Loon A, Keune K, Hermans JJ, Réfrégiers M & Berrie BH (2019). Photoluminescence micro-imaging sheds new light on the development of metal soaps in oil paintings. In *Metal Soaps in Art*. Cultural Heritage Science, Casadio F, Keune K, Noble P, Van Loon A, Hendriks E, Centeno SA & Osmond G (Eds.), pp. 211–225. Cham: Springer. [https://doi.org/10.1007/978-3-319-90617-1\\_12](https://doi.org/10.1007/978-3-319-90617-1_12).
- Van Der Snickt G, Dik J, Cotte M, Janssens K, Jaroszewicz J, De Nolf W, Groenewegen J & Van Der Loeff L (2009). Characterization of a degraded cadmium yellow (CdS) pigment in an oil painting by means of synchrotron radiation based X-ray techniques. *Anal Chem* **81**, 2600–2610.
- Van Der Snickt G, Janssens K, Dik J, De Nolf W, Vanmeert F, Jaroszewicz J, Cotte M & Falkenberg G (2012). Combined use of synchrotron radiation based micro-X-ray fluorescence, micro-X-ray diffraction, micro-X-ray absorption near-edge, and micro-Fourier transform infrared spectroscopies for revealing an alternative degradation pathway of the pigment cadmium yellow. *Anal Chem* **84**, 10221–10228.
- Vanmeert F, De Wael K, Janssens K, Falkenberg G & Cotte M (2019). Using synchrotron radiation for understanding the spontaneous degradation of artists' pigments. *Synchrotron Radiat News* **32**, 41–47.
- Vaudey CE, Gaillard C, Toulhoat N, Moncoffre N, Schlegel ML & Raimbault L (2011). Chlorine speciation in nuclear graphite studied by X-ray absorption near edge structure. *J Nucl Mater* **418**, 16–21.
- Veamatahau A, Jiang B, Seifert T, Makuta S, Latham K, Kanehara M, Teranishi T & Tachibana Y (2015). Origin of surface trap states in CdS quantum dots: Relationship between size dependent photoluminescence and sulfur vacancy trap states. *Phys Chem Chem Phys* **17**, 2850–2858.
- Xu L, Liang HW, Yang Y & Yu SH (2018). Stability and reactivity: Positive and negative aspects for nanoparticle processing. *Chem Rev* **118**, 3209–3250.